Petroleum Science 19 (2022) 1494–1504

Contents lists available at ScienceDirect

Petroleum Science

journal homepage: www.keaipublishing.com/en/journals/petroleum-science

Original Paper

A novel redox indicator based on relative abundances of C_{31} and C_{32} homohopanes in the Eocene lacustrine Dongying Depression, East China

Chong Jiang [a], Hai-Ping Huang [a, b, c, *], Zheng Li [d], Hong Zhang [b], Zheng Zhai [d]

[a] School of Energy Resource, China University of Geosciences (Beijing), Beijing, 100083, China
[b] School of Geosciences, Yangtze University, Wuhan, Hubei, 430100, China
[c] Department of Geoscience, University of Calgary, Calgary, Alberta, T2N 1N4, Canada
[d] Geology Scientific Research Institute of Shengli Oilfield Company, Sinopec, Dongying, Shandong 257015, China

ARTICLE INFO

Article history:
Received 26 June 2021
Accepted 28 October 2021
Available online 2 February 2022

Edited by Jie Hao

Keywords:
paperBiomarkers
C_{32}/C_{31} homohopane ratio
Redox conditions
Dongying Depression

ABSTRACT

A suite of oils and bitumens from the Eocene Shahejie Formation (Es) in Dongying Depression was geochemically characterized to illustrate impact of source input and redox conditions on distributions of pentacyclic terpanes. The Es_4 developed under highly reducing, sulfidic hypersaline conditions, while Es_3 formed under dysoxic, brackish to freshwater conditions. Oils derived from Es_4 are enriched in C_{32} homohopanes ($C_{32}H$), while those from Es_3 are prominently enriched in C_{31} homohopanes ($C_{31}H$). The $C_{32}H/C_{31}H$ ratio shows positive correlation with homohopane index (HHI), gammacerane index, and negative correlation with pristane/phytane ratio, and can be used to evaluate oxic/anoxic conditions during deposition. High $C_{32}H/C_{31}H$ ratio (> 0.8) is an important characteristic of oils derived from anoxic environments, while low values (< 0.8) indicate dysoxic conditions and extremely low values (< 0.4) indicate strong oxic conditions. The $C_{32}H/C_{31}H$ ratio can be applied for deposition condition diagnosis because carboxyl group of C_{32} hopanoic acids might be reduced to C_{32} homohopanes under anoxic conditions, and oxidized to C_{31} homohopane under oxic conditions. Advantages to use $C_{32}H/C_{31}H$ ratio as redox condition proxy compared to the HHI and gammacerane indexes are wider valid maturity range, less sensitive to biodegradation influence and better differentiating reducing from oxic environments.

1. Introduction

Numerous biomarker parameters are available in the literature to diagnose organic facies and depositional environments. The *n*-alkane distribution (Bray and Evans, 1961), ratio of pristane (Pr) to phytane (Ph) (Didyk et al., 1978), relative abundances of C_{27}, C_{28} and C_{29} steranes (Huang and Meinschein, 1979), occurrence of 28,30-bisnorhopane (Noble et al., 1986), C_{30} tetracyclic polyprenoids (Holba et al., 2003) and C_{30} steranes (Moldowan et al., 1985), elevated gammacerane and C_{35}-homohopane abundance (Moldowan et al., 1986; Peters and Moldowan, 1991), are commonly used indicators among many others. Hopane distributions, in particular, have been the focus of biomarker investigations for decades because of their ubiquitous occurrence in geological samples and their unique precursors in organisms and sensitivity to redox conditions at the time of sediment deposition (Mello et al., 1988; Peters et al., 2005). Hopanes are primarily derived from biochemical processes in bacteria and cyanobacteria (Ourisson et al., 1979), and their diagenetic and catagenetic evolution after burial in sediments is relatively well understood (Farrimond et al., 1998, 2003). Origin, redox condition, and thermal alteration are the three main factors controlling the final distributions of hopanes in the source rock extracts (bitumens) and related oils (Ourisson et al., 1979; Mello et al., 1988; Farrimond et al., 1998).

C_{29} 17α,21β(H) 30-norhopane ($C_{29}H$) and C_{30} 17α,21β(H) hopane ($C_{30}H$) are typically the most abundant hopane components in oils and bitumens. The relative abundance of $C_{29}H$ and $C_{30}H$ appears to be sensitive to lithological changes with $C_{29}H/C_{30}H$ ratios of > 1.0 characterizing evaporitic-anoxic carbonate source rocks, while lower values (< 1.0) indicates a clay-rich siliciclastic source (Clark and Philp, 1989; Waples and Machihara, 1990). Homohopanes ($C_{31}H$–$C_{35}H$) are generally believed to originate from bacteriohopanepolyols, which are synthesized as membrane lipids by

* Corresponding author. School of Energy Resource, China University of Geosciences (Beijing), Beijing, 100083, China.
E-mail address: huah@ucalgary.ca (H.-P. Huang).

https://doi.org/10.1016/j.petsci.2022.01.019

bacteria (Ourisson et al., 1979; Farrimond et al., 2004). The C_{35} homohopanes are selectively preserved by sulfur incorporation under anoxic conditions, while lower carbon homologs are preferentially preserved under suboxic to oxic conditions due to side chain cleavage (Sinninghe Damsté et al., 1995a; Köster et al., 1997). Dominant C_{31} homohopanes without C_{34} and C_{35} homohopanes usually indicates terrigenous plant-derived organic matter, especially in coaly strata (Wang, 2007; French et al., 2012), while the dominance of C_{33} homohopane, coupled with the elevated 28,30-bisnorhopane, may be indicative of specific bacterial input in an anoxic marine niche environment (Lerch et al., 2017). A commonly used indicator of depositional conditions of source rocks is the homohopane index [$HHI = C_{35}/\Sigma(C_{31}–C_{35})$ (22S + 22R)] (Peters and Moldowan, 1991). Bishop and Farrimond (1995) further proposed that a $C_{31}H$:$C_{33}H$:$C_{35}H$ ternary diagram, coupled with a hopane odd/even predominance parameter, is a good depiction of overall homohopane carbon number distributions. They applied the distributions of homohopanes for oil-oil and oil-source rock correlation in the North Sea. However, the causes of homohopane compositional differences and their significance in geochemical application remain poorly understood.

Generally, oils and bitumens derived from highly reducing environments of deposition contain high relative abundance of $C_{32}–C_{35}$ homohopanes, while those from freshwater lacustrine environments have low abundance of homohopanes, especially $C_{33}–C_{35}$ homohopanes (Philp et al., 1989; Fu et al., 1990). The preservation of distinctive carbon numbers of extended hopanes appears to be controlled by the availability of free oxygen during deposition (Moldowan et al., 1986). For example, the marine Triassic Filletino oil from the Adriatic Sea shows elevated C_{32} homohopane and gammacerane. However, variations of the C_{32}/C_{31} homohopane ratio in geological samples and its application to assess depositional environment has not been fully explored.

Dongying Depression in the Bohai Bay Basin, east China, is a prolific oil production province where the source rocks were deposited under variable conditions from strongly reducing, anoxic hypersaline water to relatively oxic freshwater during basin evolution. The geochemical features of source rocks and oils from this depression have been thoroughly investigated (Shi et al., 1982; Li et al., 2003; Zhang et al., 2009; Ping et al., 2019; Zhan et al., 2019; Wang and Huang, 2021), and C_{32}/C_{31} homohopane ratios show a wide range of variation in oils and source rock extracted bitumens. The purpose of the present study is to explore the geochemical significance of the C_{32}/C_{31} homohopane ratio in the determination of redox conditions during deposition of source rocks, and the factors governing the C_{32}/C_{31} homohopane ratio during thermal maturation or alteration processes.

2. Geological background

Dongying Depression, with an area of approximately 5700 km^2, is a typical half-graben lacustrine depression situated in the southeast Jiyang Sub-basin, Bohai Bay Basin, east China (Fig. 1). It is an asymmetric depression with a steeply faulted zone in the northern side and a very gentle slope in the southern side. It is bounded by several structural highs and consists of the Lijin, Minfeng, Niuzhuang and Boxing sags and a central anticline. Detailed structural evolution, sedimentary sequence, and petroleum generation and accumulation in the depression have been well documented (Allen et al., 1997; Li, 2004; Guo et al., 2012; Lampe et al., 2012). Briefly, sediments in the Dongying Depression are mainly of the Cenozoic age and can be divided into the Paleogene Kongdian (Ek), Shahejie (Es) and Dongying (Ed) formations, the Neogene Guantao (Ng) and Minghuazhen (Nm) formations and the Quaternary Pingyuan Formation. The Ek Formation was deposited unconformably on the Mesozoic and Paleozoic surface and is mainly composed of coarse clastic red beds with limited oil generation potential. The Es Formation is widely distributed and contains the most important source rocks and reservoirs in the depression. It can be further divided into four members, namely, Es_1, Es_2, Es_3, and Es_4 (from the youngest to the oldest). The Es_4 Member was formed under saline lacustrine conditions and is characterized by thick deposits of gypsum-halite, thin dolomites and oolitic limestones interbedded with calcareous shales, and organic-rich mudstones. The overlying Es_3 Member was deposited in relatively deeper water under brackish to freshwater conditions. It consists mainly of gray and dark-gray mudstone, siltstone, and sandstone intercalated with brown–gray and gray-to-black shale (Fig. 1). Both members bear high oil and gas generation potential but oils derived from each member can be geochemically distinguished (Li et al., 2003; Zhang et al., 2009; Guo et al., 2012; Lampe et al., 2012; Liang et al., 2017; Zhan et al., 2019; Wang et al., 2021).

3. Methods

Oil samples were collected from 36 production wells with most samples situated at the southern slope of the depression. The Es_3 well refers oil from the Es_3 source rocks and the Es_4 well refers oil from the Es_4 source rocks (Fig. 1c). Oils in shallow reservoir (< 1500 m) were suffered variable biodegradation influence (Wang et al., 2013), and severely biodegraded oils were excluded from the present study. Source rock samples were collected from three shale oil wells located in the Boxing (FY1), Niuzhuang (NY1) and Lijin (LY1) sags, respectively (Fig. 1). The core samples were pulverized to 80–100 mesh with a swing mill and then extracted using dichloromethane:methanol (93:7, v:v) for 72 h in a Soxhlet apparatus. Elemental sulfur was removed during the Soxhlet extraction using activated copper strips. The extractable organic matter (EOM) was determined using an in-house method. About 50 mg of EOM and/or oil was transferred to a vial, and a suite of internal standards (cholestane-d4, adamantane-d16, phenyldodacane-d30, naphthalene-d8, phenanthrene-d10 and 1,1-binaphthalene) was added, after which the sample was transferred to a polar Florisil solid phase extraction (SPE) cartridge to remove polar compounds and obtain the hydrocarbon fraction. The hydrocarbon fraction was further separated into the aromatic and saturated hydrocarbon fractions using a modified Bastow method (Bastow et al., 2007). In order to assure the accuracy, a blank and two well characterized produced oils (a heavy oil and a light oil) were processed with each batch of samples in the same way as the rock extracts/oils.

The saturated hydrocarbon fraction was analyzed using GC–MS in both selected ion monitoring and full-scan modes (SIM/SCAN) on an Agilent 7890B gas chromatograph linked to an Agilent 5977A MSD system. A DB–1MS fused silica capillary column (60 m × 0.32 mm i.d. × 0.25 μm film thickness) was used for separation. The GC oven temperature was programmed from 50 °C (1 min) to 120 °C at 20 °C/min, then increased to 310 °C at 3 °C/min, which was held for 25 min. Helium was used as the carrier gas and a constant flow rate of 1 mL/min was applied. The temperature of the injector and interface was set at 300 °C. The ion source was operated in the electron ionization (EI) mode at 70 eV. Peak identification was performed by comparisons of the retention time index and an MS standard library. Concentrations were calculated based on peak area and no response factor calibration was performed.

4. Results

4.1. Terpane distributions in oils and bitumens

The m/z = 191 mass fragmentograms of representative oil and

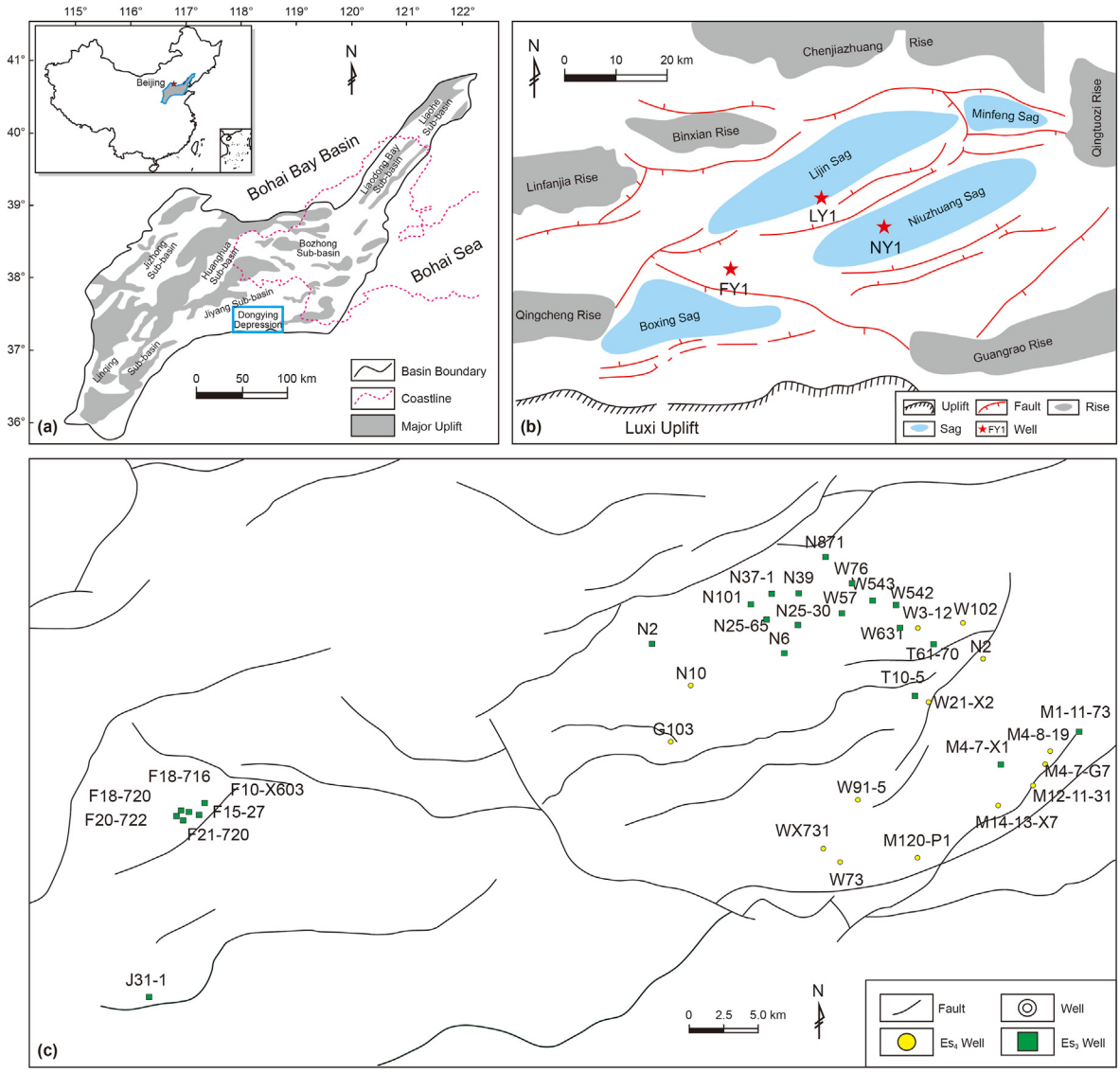

Fig. 1. Location map of study area. (**a**) Schematic map of the Bohai Bay Basin (modified after Zhang et al., 2019); (**b**) Tectonic setting map of the Dongying Depression showing the uplifts, sags, main faults and core sample locations (modified after Zhang et al., 2019); (**c**) Oil sample locations in southern part of the Dongying Depression.

bitumen samples in the saturated hydrocarbon fraction exhibit high proportions of pentacyclic terpanes (PT) relative to tricyclic terpanes (TT) (Fig. 2). The distributions of pentacyclic terpanes in all oil samples are dominated by $C_{30}H$ with a general depletion from C_{31} to C_{35} homohopanes. Minor amounts of 18α(H)-trisnorneohopane (Ts), 17α(H)-trisnorhopane (Tm), C_{29} and C_{30} 17β, 21α(H) hopanes (moretanes), C_{30} 17α(H)-diahopane ($C_{30}D$) and C_{29} 18α(H)-30-norneohopane ($C_{29}Ts$) are also present. The main difference between the Es_3 and Es_4 sourced oils is the relative abundance of homohopanes and gammacerane. The Es_3 sourced oils are characterized by relatively low concentrations of gammacerane and little or no C_{35} homohopane, showing a typical feature of freshwater lacustrine clastic source rock origin. In contrast, the Es_4 sourced oils are enriched in gammacerane and relatively high levels of C_{35} homohopane, suggesting hypersaline source rock origin.

The $m/z = 191$ chromatograms of saturated hydrocarbon fractions from representative bitumens exhibit very different features from the oils. Only samples from wells FY1 and NY1 at relatively shallow depth bear the same features as oils, while deeply buried samples from well LY1 show drastically altered pentacyclic terpanes distribution patterns. The Es_3 source rock extracted bitumens in the LY1 well show significantly depleted Tm and $C_{29}H$ and relatively concentrated Ts, $C_{29}Ts$ and $C_{30}D$, while homohopanes remain relatively constant; however, the Es_4 bitumens show substantial depletion of C_{29}–C_{35} regular hopanes with rearranged hopanes, especially Ts as a dominant peak. The C_{34} and C_{35} homohopanes are absent in a few of the deepest samples. Meanwhile, the abundance of tricyclic terpanes is relatively increased as compared to the pentacyclic terpanes (Fig. 2).

A few commonly used molecular parameters from the saturated hydrocarbon fraction in the studied samples are listed in Table 1. The $C_{32}H/C_{31}H$ ratios vary from 0.59 to 0.96 with an average value of 0.72 in the Es_3 sourced oils; whereas they range from 0.78 to 1.22 with an average value of 0.96 in the Es_4 sourced oils (Table 1). While some overlap exists between the two sourced oils likely due to mixing of charge (some known mixed oils were excluded in this study), the systematic difference in $C_{32}H/C_{31}H$ may reflect intrinsic differences in source rock depositional environment. However, the differences in bitumens are less obvious. High $C_{32}H/C_{31}H$ ratios occur only in limited samples of the Es_4 bitumens possibly due to

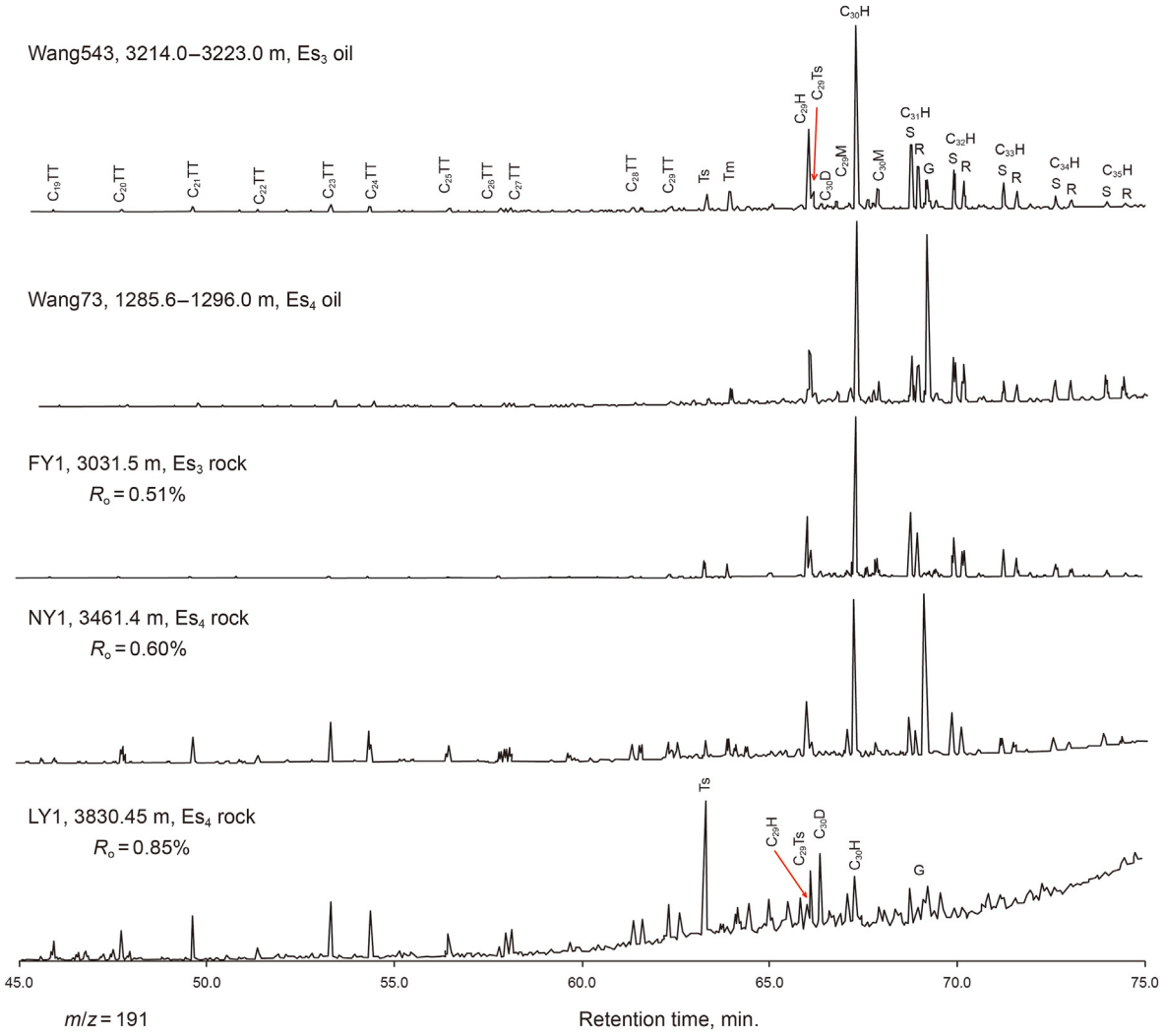

Fig. 2. The $m/z = 191$ mass fragmentograms showing terpane distributions in representative oil and bitumen samples from the Dongying Depression. C_{19}–C_{30} TT: tricyclic terpane; Ts: 18α(H)-trisnorneohopane; Tm: 17α(H)-trisnorhopane; C_{29}H: C_{29} 17α,21β(H) 30–norhopane; C_{29}Ts: C_{29} 18α(H)-30-norneohopane; C_{30}D: C_{30} 17α(H)-diahopane; C_{29}M: C_{29} 17β,21α(H) 30–normoretane; C_{30}H: C_{30} 17α,21β(H) hopane; C_{30}M: C_{30} 17β,21α(H) moretane; C_{31}–C_{35}H: C_{30}–C_{35} 17α,21β(H) homohopane; G: gammacerane.

thermal maturity influence. Fig. 3 shows diagrams that compare the $C_{32}H/C_{31}H$ ratio with other parameters that are sensitive to redox conditions and/or organic matter input. The homohopane index (HHI) values, expressed as the percent abundance of C_{35} hopanes relative to the summed C_{31} to C_{35} hopane abundances (Peters and Moldowan, 1991), for the Es_3 sourced oils are in the range of 2.9%–11.5% (average 6.3%) and those for the Es_4 sourced oils range from 7.6% to 22.4% (average 14.2%) (Table 1). The difference of HHI among the Es_3 and Es_4 bitumens is much less significant with an average value of 7.0% and 8.0%, respectively. A nearly linear correlation between $C_{32}H/C_{31}H$ ratio and HHI was observed for samples having both parameters available (Fig. 3a).

Gammacerane is present in very different concentrations in the studied samples. The gammacerane index, calculated as the ratio of gammacerane to C_{30} hopane ($G/C_{30}H$), varies between 0.04 and 0.48 in the Es_3 sourced oils and from 0.63 to 1.1 in the Es_4 sourced oils (Table 1). Lower $G/C_{30}H$ values were also observed for the Es_3 bitumens compared to the Es_4 bitumens. Positive correlation between $C_{32}H/C_{31}H$ and $G/C_{30}H$ ratios is obvious with linear correlation coefficients of 0.66 and 0.69 for the Es_3 and Es_4 sourced oils, respectively (Fig. 3b).

Most samples in the present study have phytane concentrations higher than pristane and the Pr/Ph ratio varies from 0.14 to 1.14 in all studied samples. The average Pr/Ph ratios of the Es_3 and Es_4 sourced oils are 0.55 and 0.25, respectively, while slightly higher values of Pr/Ph were observed for bitumens with an average value of 0.59 and 0.56 for the Es_3 and Es_4 source rocks, respectively (Table 1). Overall low Pr/Ph ratios suggest that Shahejie Formation source rocks are formed under reducing depositional environments. A general negative correlation between $C_{32}H/C_{31}H$ and Pr/Ph ratios occurs in the studied sample suite (Fig. 3c).

4.2. Maturity impact on terpane related parameters

Measured vitrinite reflectance ($\%R_o$) values in core samples from well NY1 are in the range of 0.44%–0.67%, and those from well FY1 and LY1 are 0.48–0.76% and 0.52–0.86%, respectively (Fig. 4a) (Ping et al., 2019; Zhang et al., 2019, 2020). While the exact value of $\%R_o$ might be suppressed due to the nature of lacustrine Type I kerogen (Guo et al., 2012), molecular ratios such as Ts/(Ts + Tm) and the ratio of tricyclic terpanes to pentacyclic terpanes (TT/PT) show good correlations with vitrinite reflectance in the studied wells. The TT/PT ratios in well NY1 vary from 0.01 to 0.35, while those from well LY1 increase from 0.1 at 3580 m to 1.14 at 3830 m (Fig. 4b). Depth profiles of Ts/(Ts + Tm) from wells NY1 and LY1 have been plotted in Fig. 4c, and this parameter increases from about 0.4 at 3300 m in

Table 1
Biomarker compositions of oils and source rock extracts from the Dongying Depression.

Well	Age	Type	Depth (m KB)	Pr/Ph	$C_{29}H/C_{30}H$	$C_{32}H/C_{31}H$	HHI	$C_{30}D/C_{29}Ts$	$G/C_{30}H$	$C_{31}R/C_{30}H$	$C_{27}St\%$	$C_{28}St\%$	$C_{29}St\%$	TT/PT	Ts/(Ts + Tm)
Jin31-1	Es_3	oil	1230.6–1254.7	0.80	0.56	0.64	5.08	0.42	0.06	0.21	29.5	30.0	40.5	0.11	0.52
Tong61-70	Es_3	oil	1796.6–1799	0.31	0.45	0.73	7.85	0.45	0.32	0.26	23.9	27.7	48.3	0.13	0.52
Wang3-12	Es_3	oil	2215–2218.2	0.36	0.44	0.74	6.93	0.23	0.28	0.24	25.8	28.5	45.7	0.11	0.49
Wang631	Es_3	oil	2775.2–2784	0.49	0.51	0.59	2.87	0.28	0.18	0.26	29.3	25.7	45.0	0.30	0.54
F15-27	Es_3	oil	2908.5–3000	1.06	0.51	0.66	5.58	0.37	0.04	0.23	32.1	28.3	39.6	0.05	0.48
F10-X603	Es_3	oil	2973–2977	1.08	0.48	0.68	6.05	0.34	0.04	0.22	29.6	31.7	38.7	0.07	0.46
F20-722	Es_3	oil	2978–2983	1.08	0.53	0.68	6.49	0.47	0.04	0.24	31.9	28.6	39.5	0.10	0.47
Niu6	Es_3	oil	2999.2–3209.6	0.30	0.46	0.87	9.85	0.35	0.48	0.25	28.7	25.5	45.8	0.11	0.47
F18-716	Es_3	oil	3109.5–3120	1.07	0.48	0.68	5.45	0.32	0.04	0.24	32.1	29.4	38.4	0.07	0.46
Niu37-1	Es_3	oil	3111.2–3125.5	0.51	0.53	0.71	6.65	0.23	0.08	0.23	27.0	30.0	43.1	0.10	0.47
F18-720	Es_3	oil	3142–3146	1.07	0.48	0.68	5.12	0.44	0.05	0.23	31.5	31.6	36.9	0.10	0.50
Wang542	Es_3	Oil	3147.4–3162.2	0.50	0.42	0.68	3.67	0.33	0.24	0.24	23.9	21.4	54.7	0.10	0.53
Niu2	Es_3	Oil	3190.4–3200.6	0.37	0.43	0.75	7.45	0.29	0.42	0.23	24.6	21.9	53.4	0.07	0.36
Wang543	Es_3	Oil	3214.0–3223.0	0.46	0.43	0.68	3.78	0.31	0.23	0.23	23.6	21.6	54.8	0.09	0.46
F21-720	Es_3	oil	3215.9–3231	0.96	0.61	0.65	5.75	0.28	0.04	0.21	32.3	28.2	39.5	0.06	0.45
Niu871	Es_3	Oil	3240.0–3290.0	0.51	0.43	0.69	4.19	0.33	0.16	0.22	24.0	20.6	55.4	0.09	0.54
Niu25-30	Es_3	oil	3254–3283.1	0.32	0.41	0.68	8.95	0.33	0.35	0.25	25.9	31.6	42.5	0.12	0.40
Niu101	Es_3	oil	3279.3–3294.3	0.35	0.50	0.69	8.02	0.38	0.16	0.25	27.1	30.2	42.7	0.10	0.43
Niu39	Es_3	oil	3279.8–3287.6	0.25	0.51	0.72	11.45	0.27	0.45	0.28	25.3	26.7	48.0	0.09	0.33
Niu25-65	Es_3	oil	3280.6–3283.3	0.29	0.51	0.76	8.95	0.23	0.29	0.22	26.6	26.6	46.8	0.12	0.43
Wang57	Es_3	Oil	3414–3415	0.49	0.43	0.68	4.22	0.29	0.18	0.26	26.8	19.8	53.4	0.08	0.51
Wang78	Es_3	Oil	3424–3436.6	0.47	0.45	0.66	4.88	0.31	0.20	0.22	25.0	20.9	54.1	0.08	0.47
M120-P1	Es_4	oil	1060–1294	0.20	0.27	1.01	16.36	0.33	0.94	0.21	28.6	29.0	42.4	0.11	0.39
M12-11-31	Es_4	oil	1080–1104	0.19	0.33	0.87	14.35	0.27	0.81	0.22	25.6	28.9	45.6	0.10	0.30
M14-13-X7	Es_4	oil	1159–1165	0.14	0.31	0.80	14.75	0.19	0.83	0.23	27.1	28.4	44.5	0.11	0.50
M4-7-G7	Es_4	oil	1173–1208	0.17	0.28	0.78	13.94	0.12	0.76	0.24	27.4	28.0	44.6	0.10	0.37
Wang73	Es_4	Oil	1285.6–1296.0	0.24	0.34	1.10	16.94	0.20	1.10	0.20	30.0	24.7	45.3	0.07	0.39
M4-8-19	Es_4	Oil	1299.6–1355.4	0.27	0.34	1.01	15.20	0.22	1.03	0.21	28.7	25.0	46.3	0.08	0.40
Wang91-5	Es_4	oil	1399–1404	0.14	0.22	1.22	22.38	0.23	1.07	0.20	30.0	28.6	41.4	0.07	0.38
WangX 731	Es_4	Oil	1656.2–1661.0	0.24	0.35	1.06	13.74	0.22	1.00	0.19	31.0	24.3	44.8	0.07	0.36
Wang21-X2	Es_4	oil	2429.5–2431.6	0.21	0.31	0.98	13.97	0.17	0.82	0.20	30.3	28.6	41.0	0.08	0.46
Niu10	Es_4	Oil	2729.0–2743.6	0.31	0.42	0.85	11.43	0.28	0.63	0.24	25.6	23.2	51.3	0.07	0.39
Wang143	Es_4	Oil	2795.4–2801.0	0.34	0.39	0.86	9.12	0.24	0.65	0.22	26.5	24.0	49.6	0.08	0.38
Wang 102	Es_4	Oil	2903.4–2952.0	0.32	0.32	1.09	14.64	0.33	1.05	0.22	27.9	23.1	49.0	0.11	0.43
Guan103	Es_4	Oil	3006–3009	0.32	0.37	0.91	14.31	0.22	0.86	0.21	26.3	23.5	50.2	0.08	0.32
Wang 587	Es_4	Oil	3458.0–3462.3	0.38	0.33	0.87	7.62	0.41	0.86	0.24	27.0	21.1	51.8	0.13	0.51
FY1	Es_3	Rock	3031.5	1.14	0.42	0.64	5.66	0.29	0.04	0.28	28.0	23.1	48.9	0.05	0.54
FY1	Es_3	Rock	3059.92	0.88	0.44	0.65	6.01	0.34	0.04	0.26	29.2	23.9	46.9	0.07	0.52
FY1	Es_3	Rock	3125.65	0.96	0.41	0.67	6.53	0.38	0.06	0.25	27.7	20.9	51.4	0.07	0.60
FY1	Es_3	Rock	3170.14	1.07	0.45	0.65	4.89	0.34	0.05	0.21	28.7	19.4	51.9	0.12	0.61
FY1	Es_3	Rock	3233.29	1.09	0.37	0.73	5.28	0.40	0.07	0.28	23.5	17.8	58.7	0.14	0.73
FY1	Es_4	Rock	3316.23	0.72	0.32	0.74	5.34	0.68	0.15	0.30	28.1	23.2	48.7	0.28	0.86
LY1	Es_3	Rock	3582.14	0.39	0.31	0.74	8.14	0.59	0.18	0.25	25.2	26.3	48.5	0.11	0.79
LY1	Es_3	Rock	3582.14	0.39	0.31	0.73	7.49	0.59	0.17	0.25	24.5	25.8	49.7	0.11	0.79
LY1	Es_3	Rock	3586.16	0.38	0.33	0.74	8.33	0.53	0.19	0.24	24.5	26.9	48.6	0.10	0.76
LY1	Es_3	Rock	3593.01	0.38	0.34	0.75	8.10	0.49	0.19	0.23	24.5	26.6	48.9	0.10	0.73
LY1	Es_3	Rock	3598.15	0.38	0.35	0.75	8.32	0.46	0.18	0.23	24.1	26.4	49.5	0.11	0.72
LY1	Es_3	Rock	3601.21	0.39	0.35	0.74	7.86	0.47	0.18	0.24	24.3	25.4	50.3	0.11	0.71
LY1	Es_3	Rock	3658.46	0.96	0.35	0.78	4.83	0.41	0.09	0.27	28.4	18.1	53.6	0.17	0.81
LY1	Es_3	Rock	3672.38	0.88	0.34	0.75	4.98	0.44	0.10	0.29	26.0	17.3	56.7	0.17	0.82
LY1	Es_3	Rock	3674.34	0.94	0.34	0.80	4.97	0.47	0.09	0.28	24.8	17.6	57.6	0.17	0.82
LY1	Es_3	Rock	3674.34	0.95	0.34	0.79	5.09	0.47	0.09	0.29	24.5	17.0	58.5	0.17	0.82
LY1	Es_4	Rock	3751.14	0.73	0.31	0.71	8.52	0.65	0.19	0.34	26.9	24.8	48.3	0.36	0.93
LY1	Es_4	Rock	3768.15	0.59	0.31	0.64	n/a	0.80	0.31	0.42	28.3	24.2	47.6	0.44	0.95
LY1	Es_4	Rock	3771.81	0.56	0.29	0.68	n/a	0.84	0.35	0.42	27.8	25.7	46.4	0.46	0.96
LY1	Es_4	Rock	3786.16	0.50	0.38	0.58	n/a	1.00	0.57	0.43	25.0	24.4	50.5	0.61	0.95
LY1	Es_4	Rock	3803.65	0.53	0.48	0.62	n/a	1.15	0.71	0.41	22.8	23.0	54.2	1.01	0.95
LY1	Es_4	Rock	3815.76	0.55	0.52	0.67	n/a	0.97	0.66	0.51	23.6	23.1	53.3	0.90	0.94
LY1	Es_4	Rock	3830.45	0.56	0.47	n/a	n/a	1.50	n/a	n/a	25.6	21.5	52.9	1.14	0.92
NY1	Es_3	Rock	3304.1	0.86	0.49	0.66	6.43	0.22	0.06	0.24	26.5	18.2	55.3	0.04	0.43
NY1	Es_4	Rock	3333.04	0.82	0.46	0.64	7.12	0.27	0.06	0.25	24.6	20.3	55.1	0.05	0.43
NY1	Es_4	Rock	3372.9	0.42	0.39	0.65	6.27	0.27	0.07	0.26	28.8	23.3	47.8	0.06	0.48
NY1	Es_4	Rock	3377.84	0.95	0.40	0.66	6.06	0.39	0.05	0.25	27.0	20.8	52.2	0.06	0.52
NY1	Es_4	Rock	3402.73	0.50	0.41	0.69	6.69	0.27	0.19	0.28	22.5	19.8	57.7	0.07	0.57
NY1	Es_4	Rock	3402.73	0.51	0.40	0.69	6.82	0.28	0.19	0.28	21.1	20.1	58.8	0.07	0.57
NY1	Es_4	Rock	3438.12	0.46	0.27	0.92	16.65	0.22	0.71	0.28	27.6	23.1	49.3	0.12	0.76
NY1	Es_4	rock	3461.4	0.41	0.36	1.13	9.20	0.34	1.22	0.16	26.3	25.4	48.3	0.35	0.53
NY1	Es_4	Rock	3462.58	0.27	0.28	1.12	17.45	0.28	2.16	0.29	23.0	28.9	48.1	0.16	0.72
NY1	Es_4	rock	3482.3	0.29	0.36	0.90	8.68	0.35	1.64	0.24	29.2	27.1	43.7	0.32	0.75

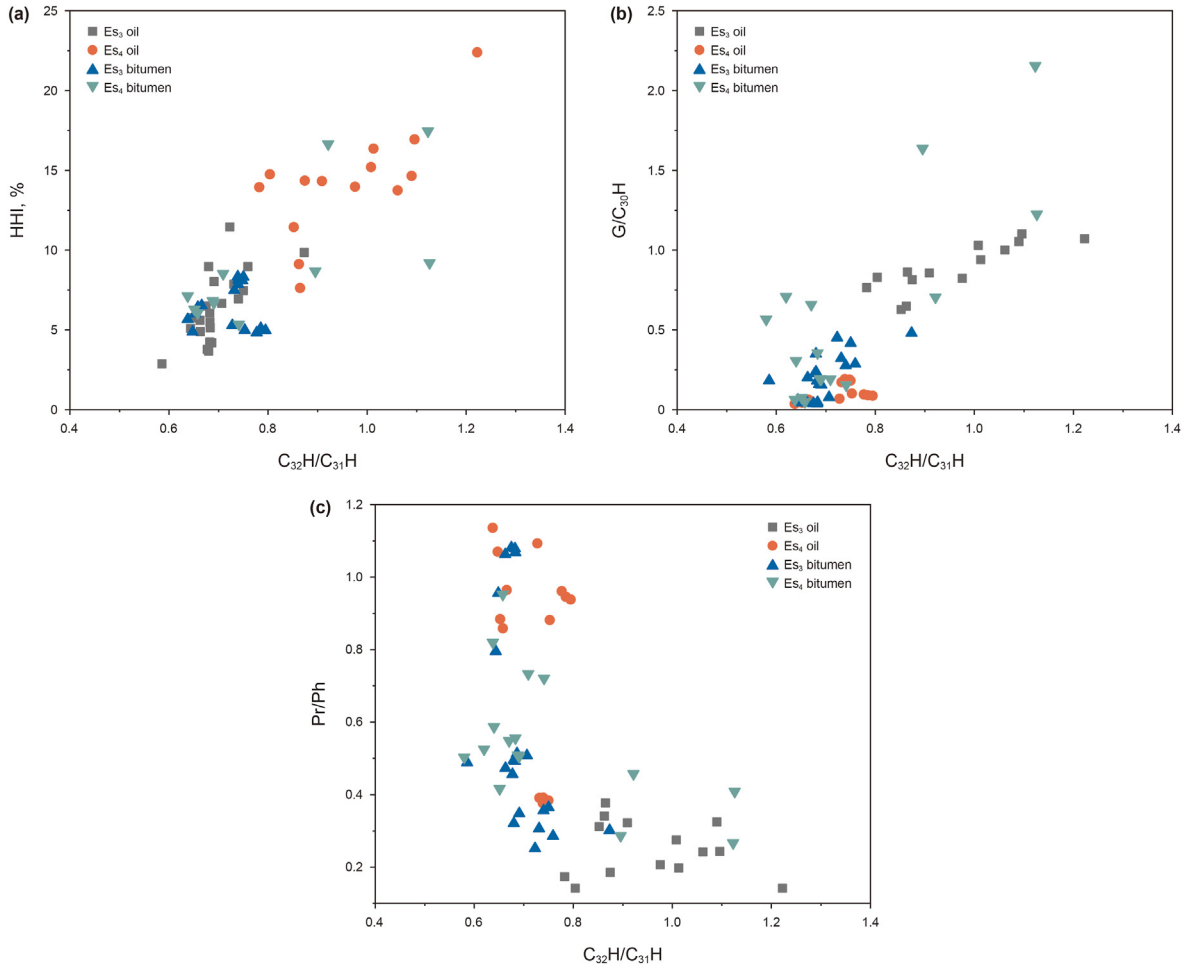

Fig. 3. Plot of $C_{32}H/C_{31}H$ ratio *vs.* known depositional environment parameters in oil and bitumen samples from the Dongying Depression. (**a**) Homohopane index (HHI); (**b**) Gammacerane index ($G/C_{30}H$); and (**c**) pristane/phytane ratio (Pr/Ph).

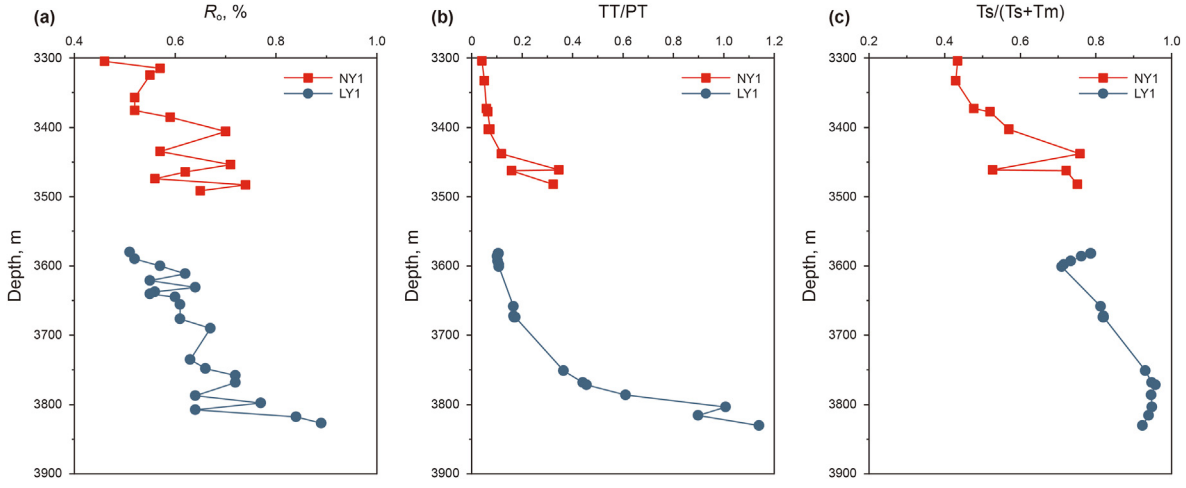

Fig. 4. Depth profile of source rock maturity in wells NY1 and LY1. (**a**) Measured vitrinite reflectance; (**b**) Concentration ratio of tri-to pentacyclic terpanes (TT/PT); (**c**) Concentration ratio of Ts/(Ts + Tm).

well NY1 to greater than 0.95 at 3800 m in well LY1. While the organic input and redox conditions have inevitably exerted some influence on TT/PT and Ts/(Ts + Tm) ratios in lacustrine source rocks, good correlation with $\%R_o$ and depth suggests that thermal maturity plays the dominant role on the variation of these ratios. The Ts/(Ts + Tm) ratios from the Es_3 and Es_4 oils are very similar within a range of 0.33–0.54 and 0.30–0.51, respectively. Similarly, all oils have TT/PT ratios below 0.15. Relatively low Ts/(Ts + Tm) and

TT/PT ratios suggest generally low maturity of oils in the Dongying Depression.

Here the TT/PT ratio has been applied as a maturity determinant for oils, because vitrinite reflectance cannot be directly measured. A plot of TT/PT and $C_{32}H/C_{31}H$ shows no correlation for the studied oils. However, elevated TT/PT ratios corresponding to low $C_{32}H/C_{31}H$ ratios occur in the bitumen samples, especially the Es_4 sourced bitumens, indicating preferential cracking of high molecular-weight homohopanes (Fig. 5a). The correlation between TT/PT ratio and HHI is also very weak. An issue for HHI is that no reliable C_{35} homohopane can be detected from some Es_4 bitumens due to high maturity (Fig. 5b). Extensive cracking of homohopanes at high maturity makes HHI unusable as a redox indicator in mature source rocks. There is no obvious correlations between TT/PT and $G/C_{30}H$ ratios in all oils and Es_3 bitumens. However, the Es_4 bitumens fall in two categories. Some samples have high $G/C_{30}H$ ratios but low TT/PT ratios, reflecting hypersaline conditions (without maturity influence), while others show linear correlation between $G/C_{30}H$ and TT/PT ratios, suggesting maturity related variation due to preferential cracking of $C_{30}H$ (Fig. 5c).

5. Discussion

5.1. Why the $C_{32}H/C_{31}H$ ratio is needed

Redox conditions are known to affect the distribution of terpanes (Peters and Moldowan, 1991). Our data from the Dongying Depression illustrate that high values of $C_{32}H/C_{31}H$ correspond with high values of HHI and $G/C_{30}H$, suggesting that $C_{32}H/C_{31}H$ is sensitive to depositional environment as well. However, HHI and gammacerane index have been applied as depositional environment indicators for decades, why the $C_{32}H/C_{31}H$ ratio is still needed. Our first concern is maturity sensitivity. The thermal maturity influence on HHI is a well-documented phenomenon. In our studied samples, no C_{34} and C_{35} homohopanes can be reliably detected in the Es_4 bitumens when R_o is > 0.75% in well LY1, which limits the utility of HHI as redox indicator. The decrease of HHI with increasing thermal maturity has also been reported in related mature oils (Peters and Moldowan, 1991; Vu et al., 2009). While maturity influence on $C_{32}H/C_{31}H$ has not been systematically documented, the mass chromatograms in the Es_4 bitumens and correlation between $C_{32}H/C_{31}H$ and TT/PT ratios in our studied samples suggest that $C_{32}H/C_{31}H$ ratio suffers similar influence as the $C_{35}H/C_{34}H$ ratio but much less dramatically. HHI was deteriorated at early oil generation stage and no reliable HHI can be obtained from source rocks R_o ~ 0.75%, while reliable $C_{32}H/C_{31}H$ ratio can be calculated up to R_o ~ 1.0% when regular hopanes are largely vanished and the $C_{32}H/C_{31}H$ ratio remains valid until R_o ~ 0.85% in the Dongying Depression. Maturity impact on homohopane distribution and the preferential depletion of the C_{35} homohopanes were well documented in the literature. Pan et al. (2008) reported the results of pyrolysis experiments performed on a source rock (YHS1) deposited in a saline environment. The samples were heated to temperatures of 180, 210, 240, 270, 300, and 320 °C

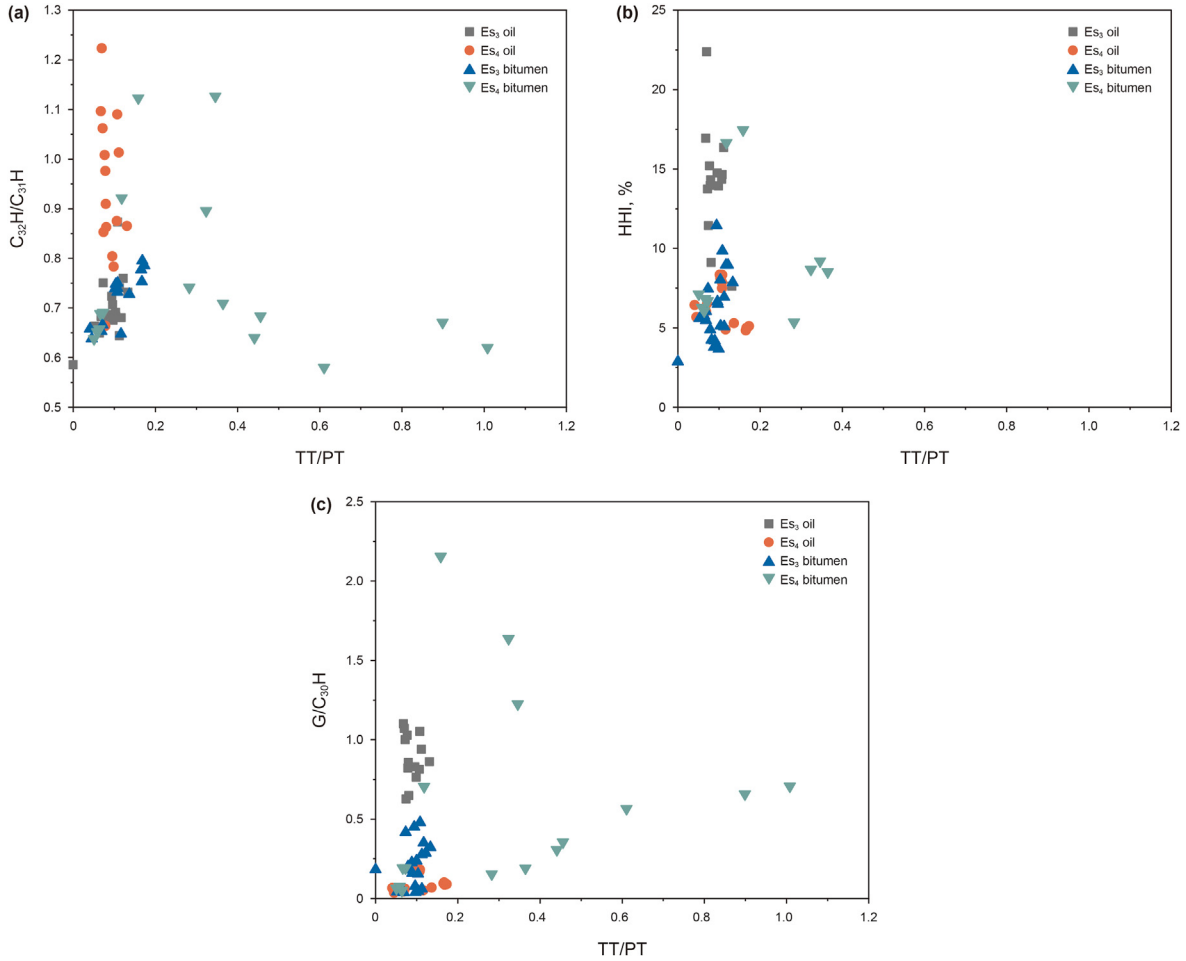

Fig. 5. Plot of summed tricyclic terpanes to summed pentacyclic terpanes (TT/PT) ratio with redox condition parameters in oil and rock samples from the Dongying Depression. (**a**) $C_{32}H/C_{31}H$ ratio; (**b**) Homohopane index; (**c**) Gammacerane index.

during 2 h and isothermally hold for 72 h in a confined system (Au capsules) under 50 MPa. The original sample shows obvious elevated C_{32} and C_{35} homohopanes with $C_{35}H/C_{34}H$ and $C_{32}H/C_{31}H$ ratios of 1.29 and 1.12, respectively. Once heated to 180 °C, the $C_{35}H/C_{34}H$ and $C_{32}H/C_{31}H$ ratios drop to 0.93 and 0.99, respectively, with 28% and 12% of reduction. The $C_{35}H/C_{34}H$ and $C_{32}H/C_{31}H$ ratios in pyrolysates at 320 °C are 0.89 and 0.82, a 31% and 26% of reduction. Hydrous pyrolysis experiments performed by Peters and Moldowan (1991) for the Monterey shale delivered the similar results. The unheated siliceous member (GC-MS No. 767) has C_{31} to C_{35} homohopanes in relative percentage of 30.8, 25.2, 17.3, 8.0 and 18.7, respectively. Once heated at 290 °C, relative percentage of C_{31} to C_{35} homohopanes becomes 38.9, 27.1, 17.6, 8.2 and 8.2, respectively. The $C_{32}H/C_{31}H$ ratio drops from 0.82 to 0.7 with 14.5% of reduction, while the HHI and $C_{35}H/C_{34}H$ ratios drop from 18.7 to 8.2 and from 2.3 to 1.0, with 56.1% and 57.2% of reduction. The pyrolysis results are consistent with our observations for the Es_4 bitumens where no reliable HHI can be obtained when TT/PT ratios are > 0.4 and $C_{32}H/C_{31}H$ ratios decrease accordingly with increasing TT/PT ratios. However, much slow reduction of $C_{32}H/C_{31}H$ ratio as compared to HHI and $C_{35}H/C_{34}H$ ratios attests a wider valid range of $C_{32}H/C_{31}H$ ratio during maturation.

High gammacerane abundance is a useful indicator of hypersalinity and/or water column stratification during deposition of sediments (Moldowan et al., 1986; Sinninghe Damsté et al., 1995b). Gammacerane mainly originates from tetrahymanol in bacterivorous ciliates living in hypersaline water (Ten Haven, 1989). High $G/C_{30}H$ ratios in the Es_4 bitumens and related oils (Table 1) reflect salinity stratification and are a marker for photic zone anoxia during source rock deposition, which is supported by the high sulfur content of the Es_4 oils (Zhan et al., 2019). Low gammacerane index values ($G/C_{30}H$ generally < 0.4) in the Es_3 bitumens and related oils indicate no stratified water or very low salinity in the palaeolake during the deposition of sediments. However, gammacerane is thermally more stable than C_{30} hopane. Once hopane thermal cracking was initiated, gammacerane index increases linearly with maturity (Fig. 5). Zhang et al. (2020) noted that some abnormally high gammacerane indexes in bitumens might be caused by preferential cracking of $C_{30}H$ and cannot be regarded as a proxy for depositional environment in the Dongying Depression. While maturity inevitably affects relative abundance of C_{31} and C_{32} homohopanes, thermal stability difference between them is less significant than the difference between $C_{30}H$ and gammacerane (Peters et al., 2005), which makes validity range of the $C_{32}H/C_{31}H$ ratio less sensitive to maturation than the $G/C_{30}H$ ratio.

The second consideration is biodegradation influence. Homohopane distributions can be altered by biodegradation. Peters et al. (1996) demonstrated that biodegradation can result in selective loss of low molecular weight homologs, while C_{35} homohopanes are more resistant. The HHI increase dramatically with the extent of biodegradation because C_{35} homohopanes are demethylated less readily than their lower homologs. Similarly, gammacerane has much higher ability to resist biodegradation than other regular hopanes and becomes the dominant component in the *m*/*z* 191 mass chromatograms of heavily biodegraded oils (Zhang et al., 2014; Huang and Li, 2017). While heavily biodegraded oils have not been selected in the present study, selective preservation of C_{35} homohopanes and gammacerane have been noted from biodegraded oils in the Dongying Depression (Wang et al., 2013). However, biodegradation preference between C_{31} and C_{32} homohopanes is much less distinctive compared to compounds in the HHI and $G/C_{30}H$. Therefore, the $C_{32}H/C_{31}H$ ratio is more robust than HHI and $G/C_{30}H$ in heavily biodegraded oils.

The third advantage to use the $C_{32}H/C_{31}H$ ratio is its sensitivity in redox conditions. High C_{35}-homohopane indices are typical of marine, low Eh environments of deposition. The elevated C_{35}-homohopanes for the lacustrine oil indicate a highly reducing source rock depositional environment, most likely related to hypersalinity during the deposition. However, in anoxic, freshwater lacustrine environments, this enhanced preservation of higher hopane homologs does not occur, probably because the appropriate mechanism for sulfur incorporation is not operative (Peters and Moldowan, 1991). Therefore, low C_{35}-homohopane index does not imply the oxic depositional system. Similarly, high gammacerane index may reflect hypersaline and strong reducing conditions in lacustrine depositional system, but low gammacerane index does not necessary reflect oxic conditions. On other hand, the $C_{32}H/C_{31}H$ ratio can differentiate reducing from oxic depositional environments in a similar manner as Pr/Ph ratio. The Pr/Ph ratio is one of the most commonly used geochemical parameters and has been widely invoked as an indicator of redox conditions in the depositional environment and source of organic matter (Didyk et al., 1978). Organic matter derived from terrigenous plants would be expected to have high Pr/Ph ratios of > 3.0 (oxic conditions), while organic matter formed under anoxic conditions normally has low Pr/Ph ratios of < 1.0 (Didyk et al., 1978). Similarly, high $C_{32}H/C_{31}H$ ratio (> 0.8) indicates reducing conditions, while low $C_{32}H/C_{31}H$ ratio (< 0.8) reflects suboxic conditions and extremely low $C_{32}H/C_{31}H$ ratio (< 0.4) is indicative of strong oxidation environment such as coal seam deposition (see further discussion in next section).

5.2. Does $C_{32}H/C_{31}H$ ratio work for other petroleum systems

The geochemical significance of the $C_{32}H/C_{31}H$ ratio as a redox proxy needs more supportive data from different environments. Here are a few case histories documented in the literature. Pan et al. (2008) reported six Oligocene lacustrine source rock samples from the Qaidam Basin, NW China. Those samples are formed under sulfidic conditions in the Ganchaigou Formation and are thermally immature near the oil generation threshold. They found that C_{31}–C_{35} homohopanes show unusual distribution patterns. In addition to high $C_{35}H/C_{34}H$ ratios ranging from 1.27 to 3.42 (average 1.91), five samples have the $C_{32}H/C_{31}H$ ratios > 1.0 with the highest value of 1.69 (average 1.31). The co-variation of the $C_{32}H/C_{31}H$ and $C_{35}H/C_{34}H$ ratios provides supportive evidence that elevated $C_{32}H/C_{31}H$ ratio (> 1.0) can reflect highly reducing environment (Fig. 6a). Gülbay and Korkmaz (2008) documented the Tertiary immature oil shale deposits in NW Anatolia, Turkey. The Miocene Beypazarı oil shale is unconformably set above the Paleocene-Eocene red-colored clastic deposits and interbedded with lignite. The Oligocene Bahçecik oil shale consists of marl, shale and tuff. Himmetoğlu and Gölpazarı oil shales are normal clastic deposits formed in the Paleocene-Eocene and Oligocene, respectively. Those oil shales are typically characterized by high hydrogen index and low oxygen index values. The relationship among HHI, $G/C_{30}H$ and $C_{32}H/C_{31}H$ explored here may further clarify the reducing intensity. Both C_{33} and C_{34} homohopanes are absent in the Himmetoğlu and Gölpazarı oil shales but C_{35} homohopanes were well preserved, whereas no C_{35} homohopanes can be detected from the Beypazarı oil shale and the C_{35} homohopanes are lower than C_{34} homohopanes in the Bahçecik oil shale (Fig. 6b). The $G/C_{30}H$ ratios in the Himmetoğlu and Gölpazarı oil shales are 0.32 and 0.31, while values for the Beypazarı and Bahçecik oil shales are 0.13 and 0.08, respectively. The $C_{32}H/C_{31}H$ ratios in the Himmetoğlu and Gölpazarı oil shales are 1.80 and 0.81, while values for the Beypazarı and Bahçecik oil shales are 0.74 and 0.42, respectively. All HHI, $G/C_{30}H$ and $C_{32}H/C_{31}H$ values suggest that Himmetoğlu and Gölpazarı oil shales were formed under stronger reducing environment than Beypazaran and Bahçecik oil shales.

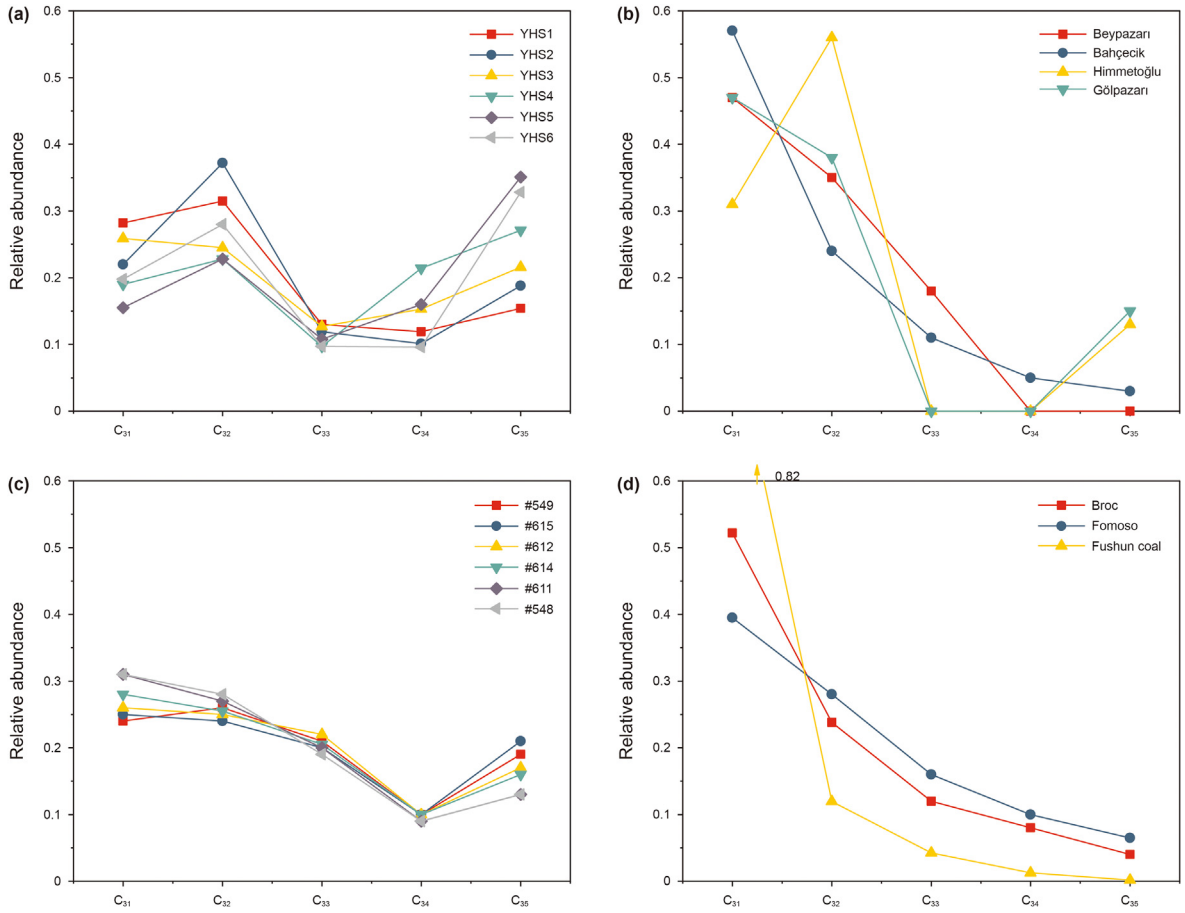

Fig. 6. Homohopane distributions for bitumen and oil samples deposited under different redox conditions. (**a**) Tertiary saline lacustrine bitumens from the Qaidam Basin (data from Pan et al., 2008); (**b**) Tertiary oil shale bitumens in NW Anatolia, Turkey (data from Gülbay and Korkmaz, 2008); (**c**) Monterey oils from offshore California (data from Peters and Moldowan, 1991); (**d**) Oxic carbonate (data of Brac and Famoso bitumens from Peters and Moldowan, 1991) and coal.

Peters and Moldowan (1991) reported a suite of Monterey oils from offshore California. The Monterey Formation was deposited in silled marine basins under highly reducing conditions without hypersalinity. The gammacerane occurs in very low abundance in these oils. The $C_{35}H/C_{34}H$ ratios in all oils are >1.0, whereas the $C_{32}H/C_{31}H$ ratios are in the range of 0.88–1.08 (average 0.95). Only one low mature sample (#549 in original paper) out of nine studied oils has $C_{32}H/C_{31}H$ ratio > 1.0 (Fig. 6c). Data from the Monterey oils may suggest that hypersalinity likely facilitates the preservation of C_{32} homohopanes, although maturity interference with the distribution of homohopanes cannot be ruled out.

ten Haven et al. (1988) studied the Messinian marl (late Miocene) formed in an evaporitic basin from Utah, USA. All samples have very low Pr/Ph ratios (< 0.1), high abundance of gammacerane, and extended hopanes maximizing at C_{35}, indicating hypersaline environments. While no relative abundance of homohopanes has been mentioned in the original paper, elevated C_{32} homohopanes with $C_{32}H/C_{31}H$ ratio > 1.0 was illustrated in the *m*/*z* 191 mass chromatograms for the Rozel Point oil (Fig. 2 in Ten Haven et al., 1988). Mello et al. (1988) studied a wide range oils from the major Brazilian offshore basins. Group III oils are characterized by a slight even/odd preference of *n*-alkanes, the predominance of phytane over pristane, high concentration of gammacerane, and $C_{35}H/C_{34}H \geq 1.0$. Inferred depositional environment for the source rock of this oil group is marine evaporitic under hypersaline conditions. Again, no $C_{32}H/C_{31}H$ ratio has been measured in the original paper, but the *m*/*z* 191 mass chromatograms for Group III oils show similar abundance of C_{31} and C_{32} homohopanes (Fig. 4 in Mello et al., 1988).

On the other hand, samples from typical oxic depositional environments have very low $C_{32}H/C_{31}H$ ratio. Peters and Molddowan (1991) used the Brac and Famoso bitumens derived from oxic carbonate sediments as a reference for HHI variation. Their $C_{35}H/C_{34}H$ ratios are 0.50 and 0.65, respectively, and $C_{32}H/C_{31}H$ ratios are 0.46 and 0.71, respectively (Fig. 6d). Both $C_{35}H/C_{34}H$ and $C_{32}H/C_{31}H$ ratios are systematically lower than these formed under highly reducing conditions. Wang (2007) recorded anomalous hopane distributions in marine sediments of the Meishan section at the Permian–Triassic boundary. While no full homohopane distribution has been documented, the $C_{32}H/C_{31}H$ ratios in 67 samples ranging from 0.38 to 0.72 (average 0.57), showing typical feature of hopanes in coals and soils. These hopanes were originated from acidified soil and peat and signified the end-Permian mass extinctions and marine ecosystem collapse (Wang, 2007). A coal from early Eocene in the Fushun Basin, North China has been illustrated in Fig. 6d for the comparison purpose. It is a low maturity coal with vitrinite reflectance about 0.5%. The C_{31} homohopanes account for 82% of extended hopanes and the $C_{32}H/C_{31}H$ ratio is only 0.15. The unusual enrichment of C_{31}-homohopanes results in extremely low $C_{32}H/C_{31}H$ ratio (< 0.4) is a defined terrigenous organic matter, especially in coals and soils under strong oxic conditions.

A plot of $C_{32}H/C_{31}H$ ratio vs. HHI using above mentioned case studies shows positive correlation, indicating that both parameters can be applied for redox condition assessment (Fig. 7). Limited data

in the present study (Fig. 4a), coupled with these published in literature, show a clear boundary between strong reducing and suboxic conditions at $C_{32}H/C_{31}H$ ratio of 0.8, whereas a boundary of redox conditions is difficult to define on the base of HHI.

5.3. Mechanisms for the $C_{32}H/C_{31}H$ ratio as a redox proxy

The mechanisms for the $C_{32}H/C_{31}H$ ratio as a redox proxy are generally similar to HHI but operate in slightly different ways. Preferential preservation of C_{35} homohopanes was attributed to the incorporation of sulfur into the bacteriohopanoid side chain during diagenesis, which mainly occurs in marine sediments formed under anoxic depositional conditions (Peters and Moldowan, 1991; Sinninghe Damsté et al., 1995a). Abnormally high HHI encountered in lacustrine saline/hypersaline sediments (Fu et al., 1990), such as the Es_4 bitumens and related oils, may share the same mechanism as the marine one, where sulfurization prevails in the organic-rich source rocks. However, this enhanced preservation of C_{35} homohopanes does not occur in freshwater sediments deposited under oxic or suboxic conditions. A narrower carbon number range of homohopane distributions commonly ranging from C_{31} to C_{33} and relatively lower HHI as illustrated by the Es_3 petroleum system indicate unique freshwater bacterial and/or terrigenous organic matter input.

The $C_{32}H/C_{31}H$ ratio is most likely controlled by the availability of free oxygen during the deposition of sediments. As homohopanes are mainly derived from bacteriohopanetetrols, diagenetic and catagenetic alteration during burial result in complex reactions including sulfurization, cyclization, side chain cleavage and condensation (Köster et al., 1997). Farrimond et al. (2003) revealed that both Priest Pot (freshwater lake) and Framvaren Fjord (sulfidic) samples released high amounts of C_{32} and C_{35} bound homohopanes by hydropyrolysis from kerogen, but the relative abundance of C_{35} homohopanes is much higher for samples from Framvaren Fjord than that from Priest Pot. The C_{30} and C_{35} are biohopanoids incorporated into the kerogen, while C_{32} hopanoic acids and hopanols are the main diagenetic products. Richnow et al. (1992) noted that oxygen-linked hopanoids showed a greater proportion of side-chain shortened homologs, which is consistent with early diagenetic products that had become incorporated into the macromolecular structure. Thiel et al. (2003) found high concentrations of free C_{32} bis-homohopanoic acids occur in microbial mats at methane seeps in anoxic Black Sea waters. All these pointed out that the C_{30}, C_{32}, and C_{35} hopanoids (mainly acids and alcohols) are primary products from biomass (mainly bacterials), while the C_{31}, C_{33}, and C_{34} are likely derived by side-chain cleavage of higher molecular weight hopanoids under different diagenetic conditions. The carboxyl group in C_{32} hopanoic acids might be reduced to C_{32}-homohopanes under anoxic conditions without the change of carbon number, otherwise, the carboxyl group would be oxidized to CO_2 and form C_{31}-homohopane if free oxygen was available (Peters and Moldowan, 1991). Therefore, the free oxygen availability plays the dominant role govern the change of $C_{32}H/C_{31}H$ ratio, which is sensitive to oxic vs. anoxic conditions for organic matter preserved in sediments and related oils. As free oxygen is typically absent in sulfidic environment, the positive correlation between $C_{32}H/C_{31}H$ ratio and HHI as illustrated in Figs. 4a and 7 is expectable.

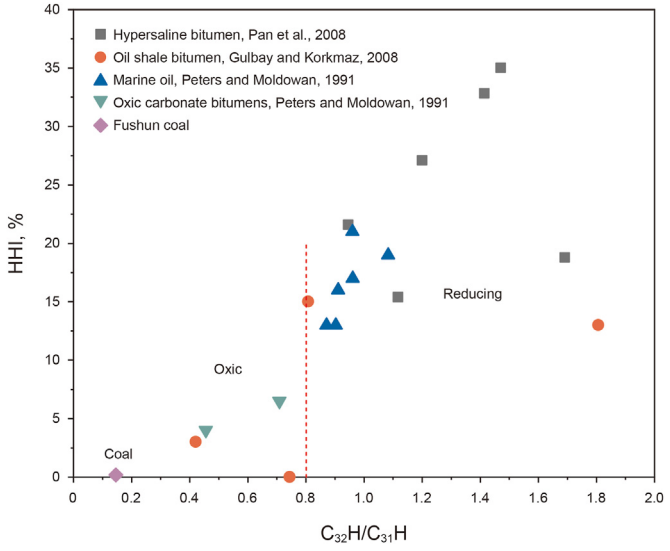

Fig. 7. Plot of HHI *vs.* $C_{32}H/C_{31}H$ showing redox condition variation.

6. Conclusions

Source rocks of the Eocene Shahejie Formation in the Dongying Depression are a result of variable depositional environments. The fourth member (Es_4) was formed under highly reducing, sulfidic and stratified hypersaline water. The bitumen and oil derived from Es_4 are characterized by high abundances of gammacerane, C_{35} homohopanes, and low Pr/Ph (< 0.5). The third member (Es_3) was formed under dysoxic, brackish to freshwater with relatively more higher-plant input and/or bacterially reworked organic matter. Bitumen and oil from the Es_3 member show distinct opposite features compared to the Es_4 counterpart.

The $C_{32}H/C_{31}H$ ratios are reasonably correlated to homohopane index (HHI), gammacerane index ($G/C_{30}H$) and Pr/Ph ratios, suggesting that $C_{32}H/C_{31}H$ can serve as a novel depositional environment proxy. High $C_{32}H/C_{31}H$ ratios (> 0.8) may indicate sulfidic, anoxic hypersaline conditions, while low ratios (< 0.8) reflect suboxic to oxic conditions in brackish to freshwater.

The mechanisms governing $C_{32}H/C_{31}H$ variation are like those for HHI, $G/C_{30}H$ and Pr/Ph but operate in slightly different ways. The availability of free oxygen during deposition likely plays a dominant role on variation of the $C_{32}H/C_{31}H$ ratio. When free oxygen is available under oxic or suboxic conditions, the precursor bacteriohopanetetrol is oxidized to a C_{32} acid, followed by loss of the carboxyl group to form the C_{31} homohopane or, if oxygen is depleted, the C_{32} homolog is preserved.

Although the $C_{32}H/C_{31}H$ ratio can be influenced by secondary alteration such as thermal cracking and biodegradation, it is more robust than HHI and gammacerane index in highly mature and heavily biodegraded oils. Meanwhile $C_{32}H/C_{31}H$ ratio is sensitive to differentiate reducing from various oxic conditions.

Acknowledgments

This work was supported by National Natural Science Foundation of China (Grant number 41873049), China Postdoctoral Science Foundation (2021M700538) and Sinopec Shengli Oilfield Drs. Steve Larter, Ken Peters, Joseph Curiale, Jian Cao and two anonymous reviewers are gratefully acknowledged for their valuable suggestions and comments that substantially improved the quality of the manuscript.

References

Allen, M.B., et al., 1997. Early Cenozoic two-phase extension and late Cenozoic thermal subsidence and inversion of the Bohai basin, northern China. Mar. Petrol. Geol. 14 (7–8), 951–972. https://doi.org/10.1016/S0264-8172(97)00027-5.

Bastow, T.P., et al., 2007. Rapid small-scale separation of saturate, aromatic and polar components in petroleum. Org. Geochem. 38 (8), 1235–1250. https://

doi.org/10.1016/j.orggeochem.2007.03.004.
Bishop, A.N., Farrimond, P., 1995. A new method of comparing extended hopane distributions. Org. Geochem. 23 (10), 987–990. https://doi.org/10.1016/0146-6380(95)00074-7.
Bray, E., Evans, E., 1961. Distribution of n-paraffins as a clue to recognition of source beds. Geochem. Cosmochim. Acta 22 (1), 2–15. https://doi.org/10.1016/0016-7037(61)90069-2.
Clark, J.P., Philp, R.P., 1989. Geochemical characterization of evaporite and carbonate depositional-environments and correlation of associated crude oils in the black creek basin, alberta. Bull. Can. Petrol. Geol. 37 (4), 401–416. https://doi.org/10.35767/gscpgbull.37.4.401.
Damste, J.S.S., et al., 1995a. Evidence for gammacerane as an indicator of water column stratification. Geochem. Cosmochim. Acta 59 (9), 1895–1900. https://doi.org/10.1016/0016-7037(95)00073-9.
Damsté, J.S.S., et al., 1995b. Early diagenesis of bacteriohopanepolyol derivatives: formation of fossil homohopanoids. Geochem. Cosmochim. Acta 59 (24), 5141–5157. https://doi.org/10.1016/0016-7037(95)00338-X.
Didyk, B., et al., 1978. Organic geochemical indicators of palaeoenvironmental conditions of sedimentation. Nature 272 (5650), 216–222. https://doi.org/10.1038/272216a0.
Farrimond, P., et al., 2003. Evidence for the rapid incorporation of hopanoids into kerogen. Geochem. Cosmochim. Acta 67 (7), 1383–1394. https://doi.org/10.1016/S0016-7037(02)01287-5.
Farrimond, P., et al., 2004. Methylhopanoids: molecular indicators of ancient bacteria and a petroleum correlation tool. Geochem. Cosmochim. Acta 68 (19), 3873–3882. https://doi.org/10.1016/j.gca.2004.04.011.
Farrimond, P., et al., 1998. Biomarker maturity parameters: the role of generation and thermal degradation. Org. Geochem. 29 (5–7), 1181–1197. https://doi.org/10.1016/S0146-6380(98)00079-5.
French, K.L., et al., 2012. Diagenetic and detrital origin of moretane anomalies through the Permian-Triassic boundary. Geochem. Cosmochim. Acta 84, 104–125. https://doi.org/10.1016/j.gca.2012.01.004.
Fu, J.M., et al., 1990. Application of biological markers in the assessment of paleoenvironments of Chinese non-marine sediments. Org. Geochem. 16 (4–6), 769–779. https://doi.org/10.1016/0146-6380(90)90116-H.
Gulbay, R.K., Korkmaz, S., 2008. Organic geochemistry, depositional environment and hydrocarbon potential of the tertiary oil shale deposits in nw Anatolia, Turkey. Oil Shale 25 (4), 444–464. https://doi.org/10.3176/oil.2008.4.05.
Guo, X.W., et al., 2012. Petroleum generation and charge history of the northern Dongying Depression, Bohai Bay Basin, China: insight from integrated fluid inclusion analysis and basin modelling. Mar. Petrol. Geol. 32 (1), 21–35. https://doi.org/10.1016/j.marpetgeo.2011.12.007.
Holba, A.G., et al., 2003. Application of tetracyclic polyprenoids as indicators of input from fresh-brackish water environments. Org. Geochem. 34 (3), 441–469. https://doi.org/10.1016/S0146-6380(02)00193-6.
Huang, H.P., Li, J., 2017. Molecular composition assessment of biodegradation influence at extreme levels - a case study from oilsand bitumen in the Junggar Basin, NW China. Org. Geochem. 103, 31–42. https://doi.org/10.1016/j.orggeochem.2016.10.005.
Huang, W.-Y., Meinschein, W., 1979. Sterols as ecological indicators. Geochem. Cosmochim. Acta 43 (5), 739–745. https://doi.org/10.1016/0016-7037(79)90257-6.
Koster, J., et al., 1997. Sulphurisation of homohopanoids: effects on carbon number distribution, speciation, and 22S/22R epimer ratios. Geochem. Cosmochim. Acta 61 (12), 2431–2452. https://doi.org/10.1016/S0016-7037(97)00110-5.
Lampe, C., et al., 2012. Fault control on hydrocarbon migration and accumulation in the Tertiary Dongying depression, Bohai Basin, China. AAPG (Am. Assoc. Pet. Geol.) Bull. 96 (6), 983–1000. https://doi.org/10.1306/11031109023.
Lerch, B., et al., 2017. Depositional environment and age determination of oils and condensates from the Barents Sea. Petrol. Geosci. 23 (2), 190–209. https://doi.org/10.1144/petgeo2016-039.
Li, P.L., 2004. Oil/gas distribution patterns in dongying depression, Bohai Bay Basin. J. Petrol. Sci. Eng. 41 (1–3), 57–66. https://doi.org/10.1016/S0920-4105(03)00143-8.
Li, S.M., et al., 2003. Geochemistry of petroleum systems in the Niuzhuang south slope of Bohai Bay Basin - part 1: source rock characterization. Org. Geochem. 34 (3), 389–412. https://doi.org/10.1016/S0146-6380(02)00210-3.
Liang, C., et al., 2017. Sedimentary characteristics and origin of lacustrine organic-rich shales in the salinized Eocene Dongying Depression. GSA Bullet. 130 (1–2), 154–174. https://doi.org/10.1130/b31584.1.
Mello, M.R., et al., 1988. Geochemical and biological marker assessment of depositional-environments using Brazilian offshore oils. Mar. Petrol. Geol. 5 (3), 205–223. https://doi.org/10.1016/0264-8172(88)90002-5.
Moldowan, J.M., et al., 1985. Relationship between petroleum composition and depositional environment of petroleum source rocks. AAPG (Am. Assoc. Pet. Geol.) Bull. 69 (8), 1255–1268. https://doi.org/10.1306/AD462BC8-16F7-11D7-8645000102C1865D.
Moldowan, J.M., et al., 1986. Sensitivity of biomarker properties to depositional environment and/or source input in the Lower Toarcian of SW-Germany. Org. Geochem. 10 (4–6), 915–926. https://doi.org/10.1016/S0146-6380(86)80029-8.
Noble, R.A., et al., 1986. Identification of some diterpenoid hydrocarbons in petroleum. Org. Geochem. 10 (4–6), 825–829. https://doi.org/10.1016/S0146-6380(86)80019-5.
Ourisson, G., et al., 1979. The Hopanoids: palaeochemistry and biochemistry of a group of natural products. Pure Appl. Chem. 51, 709–729. https://doi.org/10.1351/pac197951040709.
Pan, C., et al., 2008. Distribution and isomerization of C31–C35 homohopanes and C29 steranes in oligocene saline lacustrine sediments from Qaidam Basin, Northwest China. Org. Geochem. 39 (6), 646–657. https://doi.org/10.1016/j.orggeochem.2008.02.024.
Peters, K.E., Moldowan, J.M., 1991. Effects of source, thermal maturity, and biodegradation on the distribution and isomerization of homohopanes in petroleum. Org. Geochem. 17 (1), 47–61. https://doi.org/10.1016/0146-6380(91)90039-M.
Peters, K.E., et al., 1996. Selective biodegradation of extended hopanes to 25-norhopanes in petroleum reservoirs. Insights from molecular mechanics. Org. Geochem. 24 (8–9), 765–783. https://doi.org/10.1016/S0146-6380(96)00086-1.
Peters, K.E., Walters, C.C., Moldowan, J.M., 2005. The Biomarker Guide, second ed. Cambridge University Press, United Kingdom.
Philp, R.P., et al., 1989. An organic geochemical investigation of crude oils from Shanganning, Jianghan, Chaidamu and Zhungeer Basins, People's Republic of China. Org. Geochem. 14 (4), 447–460. https://doi.org/10.1016/0146-6380(89)90010-7.
Ping, H.W., et al., 2019. Relationship between the fluorescence colour of oil inclusions and thermal maturity in the Dongying Depression, Bohai Bay Basin, China: Part 2. fluorescence evolution of oil in the context of petroleum generation, expulsion and cracking under geological conditions. Mar. Petrol. Geol. 103, 306–319. https://doi.org/10.1016/j.marpetgeo.2019.02.024.
Richnow, H.H., et al., 1992. Structural investigations of sulfur-rich macromolecular oil fractions and a kerogen by sequential chemical degradation. Org. Geochem. 19 (4–6), 351–370. https://doi.org/10.1016/0146-6380(92)90005-I.
Ten Haven, H., et al., 1988. Application of biological markers in the recognition of palaeohypersaline environments. Geol. Soc. London, Spec. Publi. 40 (1), 123–130. https://doi.org/10.1144/GSL.SP.1988.040.01.11.
Ten Haven, H.L., et al., 1989. Tetrahymanol, the most likely precursor of gammacerane, occurs ubiquitously in marine-sediments. Geochem. Cosmochim. Acta 53 (11), 3073–3079. https://doi.org/10.1016/0016-7037(89)90186-5.
Thiel, V., et al., 2003. Unexpected occurrence of hopanoids at gas seeps in the Black Sea. Org. Geochem. 34 (1), 81–87. https://doi.org/10.1016/S0146-6380(02)00191-2.
Vu, T.T.A., et al., 2009. Changes in bulk properties and molecular compositions within New Zealand Coal Band solvent extracts from early diagenetic to catagenetic maturity levels. Org. Geochem. 40 (9), 963–977. https://doi.org/10.1016/j.orggeochem.2009.06.002.
Wang, C.J., 2007. Anomalous hopane distributions at the Permian-Triassic boundary, Meishan, China - evidence for the end-Permian marine ecosystem collapse. Org. Geochem. 38 (1), 52–66. https://doi.org/10.1016/j.orggeochem.2006.08.014.
Wang, G.L., et al., 2013. Investigation of hydrocarbon biodegradation from a downhole profile in Bohai Bay Basin: implications for the origin of 25-norhopanes. Org. Geochem. 55, 72–84. https://doi.org/10.1016/j.orggeochem.2012.11.009.
Wang, Q.R., Huang, H.P., 2021. Perylene preservation in an oxidizing paleoenvironment and its limitation as a redox proxy. Palaeogeogr. Palaeoclimatol. Palaeoecol. 562. https://doi.org/10.1016/j.palaeo.2020.110104.
Wang, Q.R., et al., 2021. Mixing scenario of a vagarious oil in the dongying depression, Bohai Bay Basin. Fuel 294. https://doi.org/10.1016/j.fuel.2021.120589.
Waples, D.W., Machihara, T., 1990. Application of sterane and triterpane biomarkers in petroleum exploration. Bull. Can. Petrol. Geol. 38 (3), 357–380. https://doi.org/10.35767/gscpgbull.38.3.357.
Zhan, Z.W., et al., 2019. Chemometric differentiation of crude oil families in the southern dongying depression, Bohai Bay Basin, China. Org. Geochem. 127, 37–49. https://doi.org/10.1016/j.orggeochem.2018.11.004.
Zhang, H., et al., 2019. Oil physical status in lacustrine shale reservoirs - a case study on Eocene Shahejie Formation shales, Dongying Depression, East China. Fuel 257. https://doi.org/10.1016/j.fuel.2019.116027.
Zhang, H., et al., 2020. Impact of maturation on the validity of paleoenvironmental indicators: implication for discrimination of oil genetic types in lacustrine shale systems. Energy Fuel. 34 (6), 6962–6973. https://doi.org/10.1021/acs.energyfuels.0c00868.
Zhang, L.Y., et al., 2009. Source rocks in mesozoic-cenozoic continental rift basins, east China: a case from dongying depression, Bohai Bay Basin. Org. Geochem. 40 (2), 229–242. https://doi.org/10.1016/j.orggeochem.2008.10.013.
Zhang, S.C., et al., 2014. Geochemistry of Paleozoic marine oils from the Tarim Basin, NW China. Part 4: paleobiodegradation and oil charge mixing. Org. Geochem. 67, 41–57. https://doi.org/10.1016/j.orggeochem.2013.12.008.